Origin of the characteristic hygro-mechanical properties of the gelatinous layer in tension wood from Kunugi oak (Quercus acutissima)

Hiroyuki Yamamoto, Julien Ruelle, Yoshiharu Arakawa, Masato Yoshida, Bruno Clair, Joseph Gril

Origin of the characteristic hygro-mechanical properties of the gelatinous layer in tension wood from Kunugi oak (*Quercus acutissima*)

Hiroyuki Yamamoto · Julien Ruelle · Yoshiharu Arakawa · Masato Yoshida · Bruno Clair · Joseph Gril

Abstract The mechanism responsible for unusual hygro-mechanical properties of tension wood containing the gelatinous layer (G-layer) was investigated. Tension and normal wood specimens were sampled from the leaning stems of a 75- and a 40-year-old Kunugi oak (*Quercus acutissima*) tree, and the moisture dependencies of the longitudinal Young's modulus and longitudinal dimensions were measured. The results, which were analyzed in relation to the anatomical properties of the specimens, revealed that the ratio of increase in the longitudinal Young's modulus with drying was higher in the G-layer than in the lignified layer (L-layer); the longitudinal drying shrinkage displayed a similar pattern. It was found that the lattice distance of the [200] plane in the cellulose crystallite increased with drying, moreover, the half-width of the [200] diffraction peak increased with drying, which was remarkable in the tension wood. Those results suggest that in the green state, the polysaccharide matrix in the G-layer behaves like a water-swollen gel; however, it is transformed into a condensed and hard-packed structure by strong surface tension during moisture desorption, which is a form of xero-gelation. However, in the L-layer, condensation and subsequent xero-gelation of the polysaccharide matrix was prevented by the hydrophobic lignin that mechanically reinforces the matrix.

Introduction

In arboreal eudicot species, tension wood xylem often produces an unusual wood fiber known as gelatinous fiber (G-fiber) along the upper sides of leaning stems or

H. Yamamoto (✉) · J. Ruelle · Y. Arakawa · M. Yoshida
School of Bioagricultural Sciences, Nagoya University, Chikusa, Nagoya 464-8601, Japan
e-mail: hiro@agr.nagoya-u.ac.jp

B. Clair · J. Gril
Laboratoire de Mecanique et Genie Civil, Universite Montpellier 2, Pl. E. Bataillon, cc 048, 34095 Montpellier Cedex 5, France

branches. The G-fibers form a gelatinous layer (G-layer) as the innermost layer of the multilayered cell wall, characterized by the absence of lignin and a high concentration of rigid cellulose microfibrils aligned along the fiber axis (Onaka 1949).

G-fibers generate high tensile growth stress during the maturation process (Okuyama et al. 1990, 1994; Yamamoto et al. 1992, 1993, 2005; Yoshida et al. 2002; Clair et al. 2003, 2008; Yamamoto 1998, 2004; Fang et al. 2008), which enables hardwood species to perform negative-gravitropic behavior in inclined shoots (Wilson and Archer 1979; Yoshida et al. 2000; Yamamoto et al. 2002). However, in timber production, tension wood is often the source of various problems, such as processing defects caused by its abnormal growth stress (Kubler 1987; Okuyama et al. 2004). Other particularities are a high longitudinal Young's modulus and a high longitudinal drying shrinkage (Yamamoto et al. 1992, 2005; Clair et al. 2003; Abe and Yamamoto 2007), the combined effect of which causes serious complications during the drying process, such as distortion and longitudinal cleavage of the sawn lumber.

Some studies have suggested that the distinctive properties of G-fibers could be attributed to the intrinsic behavior of the G-layer (e.g., Okuyama et al. 1990, 1994; Yamamoto 2004; Yamamoto et al. 1992, 2005; Clair and Thibaut 2001; Clair et al. 2003, 2006), while others have emphasized the role of the lignified layer (L-layer), which often peels off the G-layer along the same direction during microtoming (Norberg and Meier 1966; Panshin and de Zeeuw 1971; Boyd 1977). Recently, Clair et al. (2005a) noted that detachment of the G-layer, often observed in the microtomed surface of a fresh block, disappeared at a distance greater than 100 μm from the block surface, which was embedded in resin after being oven-dried. They concluded that the G-layer is strongly bound to the L-layer, even in oven-dried specimens. This finding supports the view that the intrinsic property of the G-layer is the source of the characteristic behavior of G-fibers. However, the generation mechanism of the G-layer properties is still unknown.

In the present study, the authors focused on the moisture-dependent changes in the longitudinal Young's modulus and longitudinal shrinkage in tension wood of Kunugi oak (*Quercus acutissima*), revealing the property difference between the G-layer and L-layer. Moreover, the effect of moisture desorption on the behavior of cellulose crystallites in the G-layer and L-layer was measured. Based on the obtained results, an attempt was made to elucidate the microscopic behaviors of the cellulose microfibril in drying gelatinous layer (G-layer).

Materials and methods

Sampled trees

The studied specimens were two Kunugi oaks (*Quercus acutissima*), a 75-year-old tree (Kunugi A) and a 40-year-old tree (Kunugi B), growing in a hardwood brush at the Higashiyama Campus of Nagoya University, Nagoya, Japan. The girths at chest

height were 103 cm (Kunugi A) and 73 cm (Kunugi B); both trees had inclined stems.

Measurements of the longitudinal Young's modulus and drying shrinkage at the macroscopic level

Specimens

Thin blocks were prepared from 10 or 11 points around the circumference of each stem at chest height. Sampling was done in early December. Each block was kept in fresh water at a temperature of 4°C to avoid drying. A few days later, they were cut for tensile and shrinkage tests at macroscopic level, with specimen size of 70 (Longitudinal, L) × 10 (Tangential, T) × 4 (Radial, R) and 50 (L) × 13 (T) × 5 (R) mm^3, respectively.

Measurement of longitudinal Young's modulus (E_L) at the macroscopic level

Tensile tests at macroscopic level were performed under green and oven-dried conditions in the temperature controlled room (20°C).

After the tensile test in green condition, the specimen were gradually seasoned inside air-conditioned desiccators containing successively pure water (nominal relative humidity (RH) ≈ 100%), a saturated solution of NaCl (RH 75 ± 1%), and P_2O_5 powder (RH less than 1%), in the temperature controlled room (20 ± 1°C) until the specimen reached equilibrium at each relative humidity. Finally, each specimen was oven-dried for 24 h at 105°C, and the tensile test in oven-dried state was carried out after cooling down. For each specimen, two strain gauges were bonded at the center of the flat-sawn surfaces and connected to the strain meter (Kyowa, UCAM-1A). Tensile test was performed by using commercial equipment (Imada, Type-SH-10). The outputs from both strain gauges were collected and averaged. The macroscopic longitudinal Young's modulus (E_L) at each moisture condition was determined below the proportional limit of the stress–strain curve.

Measurement of longitudinal drying shrinkage (α_L) at the macroscopic level

After measuring the longitudinal dimension in green condition, the specimens were gradually seasoned in the same manner as for the Young's modulus. Finally, the longitudinal dimension in oven-dried condition was measured. A hand-made comparator with a high precision dial gauge (0.001 mm in accuracy) was employed for the measurement of the dimension of the specimen (Yamamoto et al. 1992; Abe and Yamamoto 2006). Thus, macroscopic oven-dried shrinkage (α_L) was calculated as

$$\alpha_L = \frac{l_{\text{wet}} - l_{\text{dry}}}{l_{\text{wet}}} \times 100(\%), \tag{1}$$

where l_{wet} and l_{dry} are the longitudinal dimensions of the macroscopic specimen in the green condition and under the oven-dried condition, respectively.

X-ray diffraction properties of cell wall cellulose

Specimen

From both the heavy tension and opposite wood (normal wood) regions in Kunugi A, a sample block was taken, and kept in fresh water so as to avoid drying at a temperature of 4°C. After a few days, two types of specimen were prepared, flat-sawn sections [15 (L) × 10 (T) × 0.2 (R) mm^3] and coarse sawdust powder with a grain size of 60–35 meshes. For the flat-sawn sections, eight specimens were prepared from extra-porous zones in both the tension and normal wood blocks to offset a possible error arising from the sampling position in each block. For the sawdust powders, sufficient amounts of powder were prepared and fully stirred to become uniform.

Those samples were seasoned inside a small air-conditioned desiccator with water until equilibrium so as to remove liquid water that remarkably increases a halo peak in the X-ray diffraction diagram. The powder sample was packed into the plate-like specimen holder by hand before seasoning. The moisture condition of the samples in this stage was regarded as the fiber saturation point (FSP) in the present study, and they were used for diffraction analysis at the FSP with the reflection technique using an X-ray diffractometer (Shimadzu, XD-D1w). Samples were then air-dried inside an air-conditioned desiccator with a saturated solution of NaCl at room temperature until equilibrium and X-ray measurements were retaken, followed by oven-drying for 24 h at 105°C after seasoning inside a desiccator with a powder of P_2O_5 and further measurements. In order to prevent changes in the moisture content during X-ray measurement, moisture-conditioned air was always circulated through the sample cell (Abe and Yamamoto 2005).

Measurements of width of a single crystallite (WSC) and lattice distance from [200] plane (d_{200})

CuKα was used as a line-focused incident X-ray with a power of 35 kV, 35 mA, and passed through a Ni filter. The intensity curves, digitized and corrected for air scattering, polarization, and Compton scattering, and normalized into electron units, were used as input data for the computer program (Abe and Yamamoto 2005).

For flat-sawn sections, diffraction intensity was recorded in the 2θ angular range from 5° to 40° to determine the half width of the [200] diffraction peak (β) that was transformed into width of a single fibrous crystallite (*WSC*) in a direction perpendicular to the [200] plane under various moisture conditions. In addition, the diffraction intensities from the powder samples were recorded in the 2θ angular range from 20° to 25° to determine the peak angle from the [200] lattice plane ($2\theta_{200}$) under various moisture conditions with a high accuracy. In this measurement, three powder samples were prepared for each of tension wood and normal

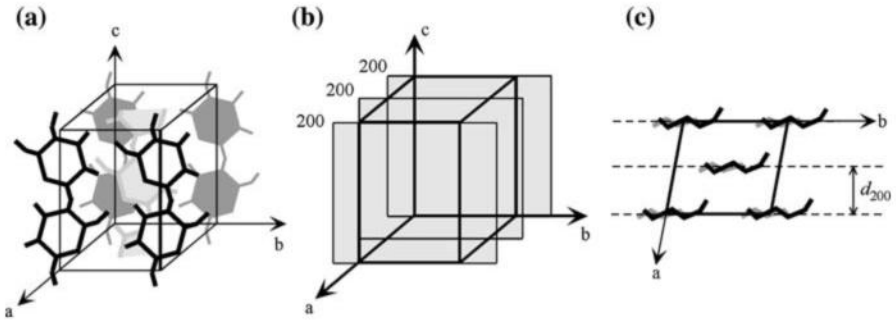

Fig. 1 Geometrical shape of unit cell of natural cellulose crystallite and its [200] plane. **a** Unit cell of natural cellulose crystallite. **b** [200] lattice plane in a unit cell. **c** Cross-section of the unit cell normal to *c*-axis, and lattice distance in [200] (=d_{200})

wood, while one sample for isolated G-layer powder that was prepared from a heavy tension wood block using the technique described by Norberg and Meier (1966). Geometrical shape of natural cellulose crystallite and its [200] lattice plane were given as displayed in Fig. 1.

In addition to those measurements, diffraction intensities from native cellulose powder (Avicell), normal wood powder, tension wood powder, and isolated G-layer powder were measured in the 2θ angular range from 5° to 40° to compare the typical X-ray diffractogram under air-dried condition.

The *WSC* value was estimated from flat-sawn sections based on the study of Hengstenberg and Mark (1928) using the modified Scherrer's equation:

$$WSC = \frac{K \cdot \lambda}{\beta \cdot \cos \theta_{200}} (\text{nm}), \tag{2}$$

where K is a constant (in the present study, $K = 1$ was assumed), λ is the wavelength of Cu Kα (=0.154 nm), β is the half-width of the [200] diffraction peak, and θ_{200} is the peak position from the [200] plane.

The value of d_{200} was determined from powder samples based on Bragg's equation:

$$d_{200} = \frac{\lambda}{2 \sin \theta_{200}} (\text{nm}). \tag{3}$$

Anatomical properties of xylem tissue

After the Young's modulus and drying shrinkage measurements, a small block was sampled from each specimen and kept in a small vial container with water for 1 month. A transverse section, 12 μm in thickness, was cut from each block on a sliding microtome and stained with safranin and fast green. After staged dehydration with ethanol and xylene, the section was mounted on a glass slide using Entellan New (Merck, Darmstadt, Germany).

Microscopic images at high and low magnification were recorded within the outermost annual rings of the mounted section under a light microscope connected

to an image processor. Macroscopic xylem consists of domains of three ligno-cellulosic tissues, that is, vessel elements including the vasicentric parenchymae, ray parenchymae, and wood fiber. From the low magnification images, the areal composition of each domain in cross section, for example, vessel elements including the vasicentric parenchymae (V), ray tissue (R), and wood fiber (F), was computed. The areal ratio of the G-fiber in the domain of wood fiber (ϕ) was also measured. From high magnification images, the ratios of the G-layer (g), L-layer (l), and total cell wall (w) areas in the domain of wood fiber were determined. Moreover, the areal ratios of the G-layer (γ) and L-layer (λ) in wood-fiber cell wall were also calculated. The relationships between the anatomical parameters were as follows: $V + R + F = 1$, $g + l = w$, and $\gamma + \lambda = 1$.

Measured values of ϕ and γ play important roles when the mechanical properties of the G-fiber and the G-layer are predicted based on the formulas 6 $\sim$ 9. By the way, a recent observation by Clair et al. (2005b) showed that transverse sectioning using a microtome blade causes an artifactual swelling in the crosscut shapes of the G-layer, which possibly caused overestimation of the g and γ values leading to underestimation of the differences in the mechanical properties between the G-layer and the L-layer. This problem will be discussed in the following chapter.

Modeling the relationship between the behavior of the wood fiber or the cell wall, and the properties of macroscopic wood

Macroscopic xylem consists of three ligno-cellulosic elements, that is, the wood-fiber domains, ray tissue, and the vessel system, including the vasicentric parenchymae. These tissues are arranged in a row in a direction parallel to the wood-fiber axis; therefore, the simple law of mixture gives the following formulae to estimate the longitudinal Young's modulus (E_L^F) and longitudinal drying shrinkage (α_L^F) of the wood-fiber domain in each specimen (Yamamoto et al. 2005):

$$E_L^F \cong E_L/F \quad \text{and} \tag{4}$$

$$\alpha_L^F \cong \alpha_L, \tag{5}$$

assuming that the vessel and ray tissues are not involved in determining the axial elasticity and axial shrinkage of the xylem.

The wood-fiber domain is composed of two types of slender, thick-walled fibers—gelatinous (G-fiber) and normal fibers (N-fiber)—arranged in rows in a direction parallel to the wood-fiber axis. In previous works by Clair et al. (2003) and Yamamoto et al. (2005), the simple law of mixture was applied to relate the longitudinal properties in a macroscopic wood with fiber properties. Then the following equations were used:

$$E_L^F = \phi \cdot E_L^g + (1-\phi)E_L^n \quad \text{and} \tag{6}$$

$$\alpha_L^F (\cong \alpha_L) = \frac{\phi \cdot E_L^g \cdot \alpha_L^g + (1-\phi) \cdot E_L^n \cdot \alpha_L^n}{\phi \cdot E_L^g + (1-\phi)E_L^n}, \tag{7}$$

where E_L^g and E_L^n are the Young's modulus of the G- and N-fiber, respectively, and α_L^g and α_L^n are their respective drying shrinkages.

The cell wall of the wood fiber consists of G- and L-layers, which are also arranged in rows parallel to the wood-fiber axis. The simple law of mixture now gives the following equations:

$$E_L^W = \gamma \cdot E^{\mathrm{G}} + (1-\gamma)E^{\mathrm{S}} \quad \text{and} \tag{8}$$

$$\alpha_L^W (\cong \alpha_{\mathrm{L}}) = \frac{\gamma \cdot E^{\mathrm{G}} \cdot \alpha^{\mathrm{G}} + (1-\gamma) \cdot E^{\mathrm{S}} \cdot \alpha^{\mathrm{S}}}{\gamma \cdot E^{\mathrm{G}} + (1-\gamma) \cdot E^{\mathrm{S}}}, \tag{9}$$

where E_L^W ($=E_L^F/w$) is the substantial Young's modulus of the cell wall along the fiber axis, and α_L^W ($\approx \alpha_L^F$) is the drying shrinkage of the cell wall in the direction parallel to the fiber axis. E^{G} and E^{S} are the Young's modulus of the G-layer along the direction of the fiber and that of the L-layer, respectively, and α^{G} and α^{S} are their respective shrinkages.

The values of E_L^g and E_L^n in the green and the oven-dried specimen were determined by applying the least square method using Eq. 6 to the observed relationship between E_L^F and ϕ. The values of α_L^g, α_L^n, and r ($=E_L^g/E_L^n$) in Eq. 7 were also determined from the observed relationship between α_L^F and ϕ on the basis of the non-linear least square method using Eq. 7. In the same manner as those cases, E^{G}, E^{S}, α^{G}, α^{S}, and s ($=E^{\mathrm{G}}/E^{\mathrm{S}}$ in Eq. 9) were determined from the observed relations between E_L^W, α_L^W, and γ through the least square method using Eqs. 8 and 9.

Results

Young's moduli of the fibers and layers (Fig. 2)

Figure 2a and b show the relationships between ϕ and E_L^F ($\approx E_L/F$) and between γ and E_L^W, respectively, under the different moisture conditions. Estimated values of E_L^g, E_L^n, E^{G}, and E^{S} are displayed in Table 1. The measured values of E_L^F were quite different between two sampled trees as shown in Fig. 2a; and estimated values of E_L^g and E_L^n were also different between them. This is because the cell wall of the wood fiber in Kunugi B was quite thicker than that in Kunugi A. After eliminating the effect of cell-wall thickness, those differences became smaller as shown in Fig. 2b and Table 1.

As a result of drying from green to oven-dried condition, the Young's modulus in L-layer (E^{S}) increased by 22.1% in Kunugi A and 29.7% in Kunugi B. Those values are in close agreement with values reported previously for spruce (Kollmann and Krech 1960) and Japanese cedar (Kojima and Yamamoto 2004). On other hand, the Young's modulus of G-layer increased considerably with the drying process at a ratio of 204.6% in Kunugi A and 80.4% in Kunugi B.

Drying shrinkage of fibers and layers from green to oven-dried condition

Figure 3a and b show the relationship between ϕ and α_{L} ($\approx \alpha_L^F$) and between α_L and γ, respectively, under different moisture conditions. From the non-linear least squares approximation using the convex hyperbolae 7 and 9, the values of α_L^g, α_L^n,

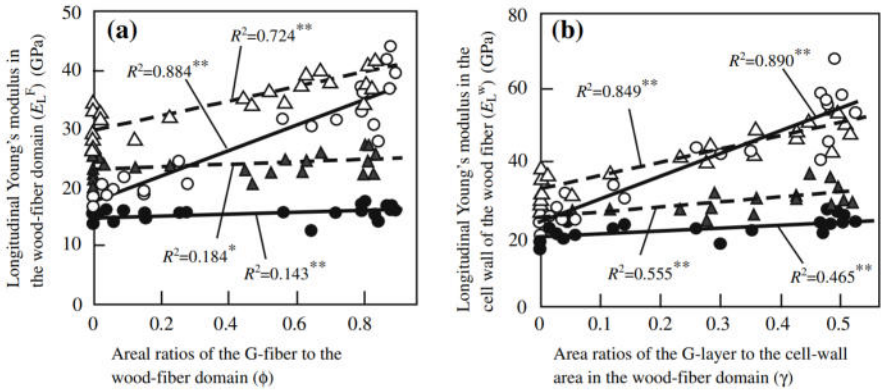

Fig. 2 **a** Relationships between the longitudinal Young's modulus in the wood-fiber domain (E_L^F) and the areal ratio of the G-fiber to the area of the wood-fiber domain (ϕ). **b** Relationships between the longitudinal Young's modulus in the cell wall of the wood fiber (E_L^W) and the area ratio of the G-layer to the area of the cell wall in the wood-fiber domain (γ). R^2 stands for contribution ratio in each regression line. *Filled circle* Kunugi A (green), *open circle* Kunugi A (oven-dried), *filled triangle*; Kunugi B (green), *open triangle*; Kunugi B (oven-dried)

Table 1 Young's moduli of the fibers and layers determined based on the linear regression analysis from Fig. 2

	Kunugi (A)		Kunugi (B)	
	Green	Oven-dried	Green	Oven-dried
Fiber Young's modulus (GPa)				
E_L^g	15.98 (±0.84)	39.16 (±2.26)	25.02 (±1.40)	41.64 (±2.23)
E_L^n	14.79 (±0.60)	17.70 (±1.61)	22.79 (±1.01)	29.52 (±1.61)
Layer Young's modulus (GPa)				
E^G	27.88 (±9.94)	84.92 (±7.04)	38.10 (±4.02)	68.73 (±5.22)
E^S	19.49 (±1.04)	23.79 (±2.50)	24.86 (±1.51)	32.24 (±1.96)

±95% confidence interval of the mean value

α^G, and α^S were determined as displayed in Table 2. As a result of drying from green to oven-dried condition, the L-layer contracted in the direction parallel to the fiber axis by 0.293% in Kunugi A and 0.058% in Kunugi B. On other hand, the G-layer contracted by 1.108% in Kunugi A and 1.122% in Kunugi B being considerably higher than the L-layer in each tree.

X-ray diffraction properties in TW cellulose

Figure 4 shows X-ray diffractograms of various powder samples in the 2θ angular range from 5° to 40° under air-dried conditions. The diffractogram of the isolated G-layer (c) was almost identical to that of Avicel powder (a), which suggests that the G-layer contains large amounts of native cellulose crystallites. The diffractogram of normal wood (b) showed a typical pattern of ligno-cellulosic material where

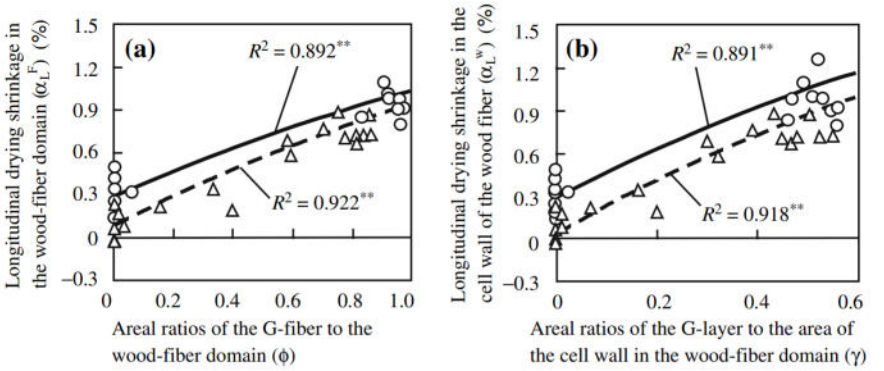

Fig. 3 **a** Relationships between longitudinal drying shrinkage (from green to oven-dry) in the wood-fiber domain (α_L^F) and areal ratio of the G-fiber to the wood-fiber domain (ϕ). **b** Relationships between longitudinal drying shrinkage in the cell wall of the wood fiber [α_L^w ($\approx \alpha_L$)] and areal ratio of the G-layer to the area of the cell wall in the wood-fiber domain (γ). R^2 stands for contribution ratio in each regression line. *Open circle* kunugi A, *open triangle* kunugi B

Table 2 Drying shrinkage of fibers and layers (from green to oven-dry) determined based on the non-linear regression analysis from Fig. 3

	Kunugi (A)	Kunugi (B)
Fiber shrinkage (%)		
α_L^g	1.000 (±0.085)	0.914 (±0.081)
α_L^n	0.294 (±0.083)	0.058 (±0.056)
r ($=E_L^g/E_L^n$)	2.177	1.200
Layer shrinkage (%)		
α^G	1.108 (±0.100)	1.122 (±0.108)
α^S	0.293 (±0.083)	0.058 (±0.058)
s ($=E^G/E^S$)	4.663	2.071

±95% confidence interval of the mean value

the peak separation between [1$\bar{1}$0] and [110] was unclear. The diffraction of tension wood powder (d) gave a similar pattern as the G-layer (c), which shows that tension wood contains a large number of G-layers. The presence of G-layer in tension wood specimen was also confirmed by the photo-microscopic observation as shown in Fig. 5. However, there were minor differences in the diffractograms between the G-layer and the tension wood powders, such as no-peak of [102] and a smaller peak of [004] in the tension wood. The reason possibly comes from the fact that the wood powder used in the present study contains a certain amount of coarse and fibrous sawdust grain, therefore, their longitudinal axis often tends to line in parallel to the surface of the plate-like specimen.

Figure 6a shows the half width of the [200] diffraction peak (β) in normal and tension wood sections under various moisture conditions. Figure 6b shows the ratios of increase in β calculated on the basis of β at the FSP. The value of β tended to increase with drying, which was noticeably higher in the tension wood than in the normal wood. Figure 7a shows values of *WSC*, calculated from Eq. 2, in normal and tension wood sections under various moisture conditions. Figure 7b shows the ratios of increase in *WSC* calculated on the basis of *WSC* at the FSP. Figure 7 indicates

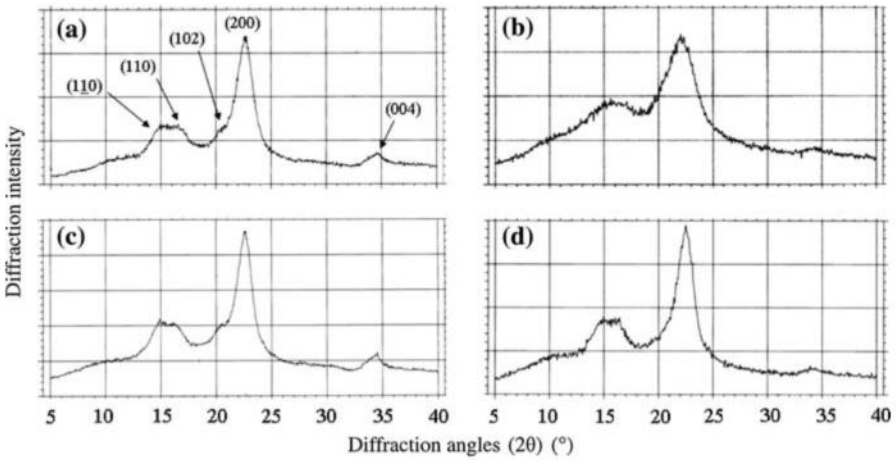

Fig. 4 X-ray diffraction patterns from **a** native cellulose powder (Avicell), **b** Kunugi normal wood powder, **c** isolated G-layer powder from Kunugi tension wood, and **d** Kunugi tension wood powder. The measurements were done in the air-dried condition

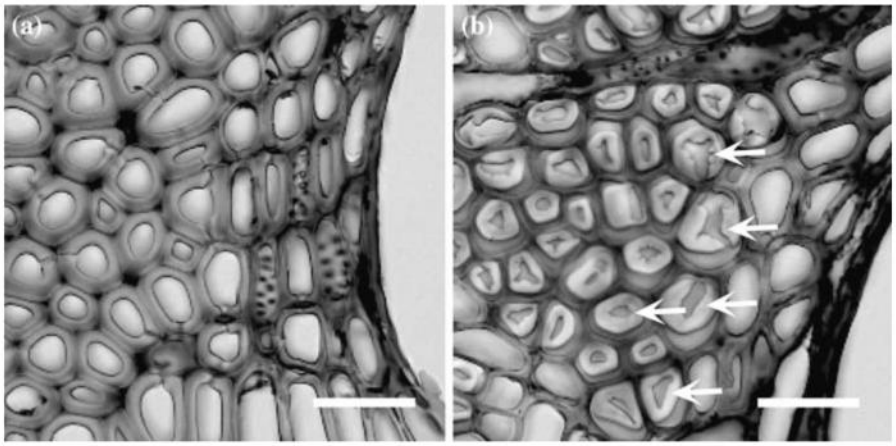

Fig. 5 Light microscopic appearances of cross-sections of **a** normal wood and **b** tension wood from Kunugi A. *Arrows* indicate the gelatinous layer (G-layer) in the tension wood fiber. *Scale bar* is 20 μm. In the tension wood specimen, it can be observed that the gelatinous layer is often peeled off from the lignified layer

that the *WSC*s in the normal and tension wood sections decreased with drying, with the ratio of decrease being higher in the tension wood (9.06%) than in the normal wood (3.05%).

Figure 8a shows the lattice distance in the [200] plane (d_{200}) in normal and tension wood powders under various moisture conditions; Fig. 8b shows the ratios of increase in d_{200} on the basis of d_{200} at the FSP. The values of d_{200} increased as the drying proceeded, and the ratios of increase from FSP to oven-dry were more or less

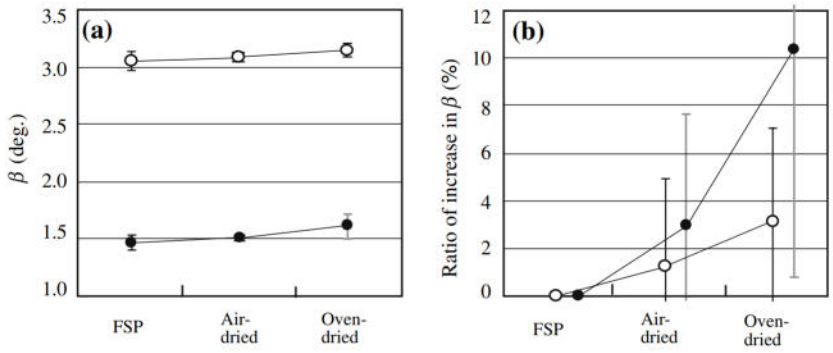

Fig. 6 **a** Half width of [200] peak (β) in normal and tension wood of Kunugi flat-sawn sections under various moisture conditions. **b** Changes in the ratio of increase of β in normal wood and tension Kunugi wood sections, calculated on the basis of β at the FSP. The *error bar* denotes ± standard deviation of eight samples. *Solid circles* average values for tension wood sections, *open circles* average values for normal wood sections (in this case, standard deviation was quite small)

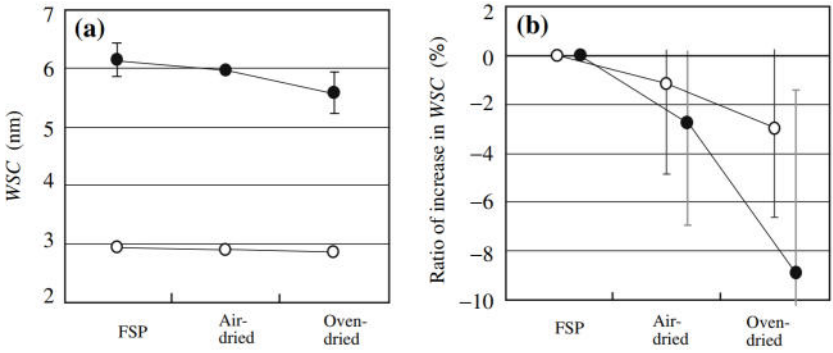

Fig. 7 **a** Width of a single crystallite in the direction perpendicular to the [200] plane (*WSC*) in normal and tension wood of Kunugi flat-sawn sections under various moisture conditions. **b** Moisture-dependent changes in the ratio of increase in *WSC* in normal and tension wood of Kunugi sections, calculated on the basis of *WSC* at the FSP. The *error bar* denotes ± standard deviation of eight samples. *Solid circles* average values for tension wood sections, *open circles* average values for normal wood sections (in this case, standard deviation was quite small)

identical in both woods (1.88% in the tension wood, and 1.77% in the normal wood).

By the way, Nishimura et al. (1981) pointed out the possibility that the moisture content change affects the scattering pattern of amorphous substance, and shifts the peak position of [200] lattice plane higher towards 2θ with increase in the moisture content. Abe and Yamamoto (2005) investigated the effect of change of scattering pattern from amorphous substance on the apparent peak position from [200] lattice plane in softwood powder as it dries. Based on the experiment in conjunction with numerical simulation, they concluded that apparent peak position of [200] decreases by 0.54° during drying, of which 0.048° were the effect of bound water in the cell

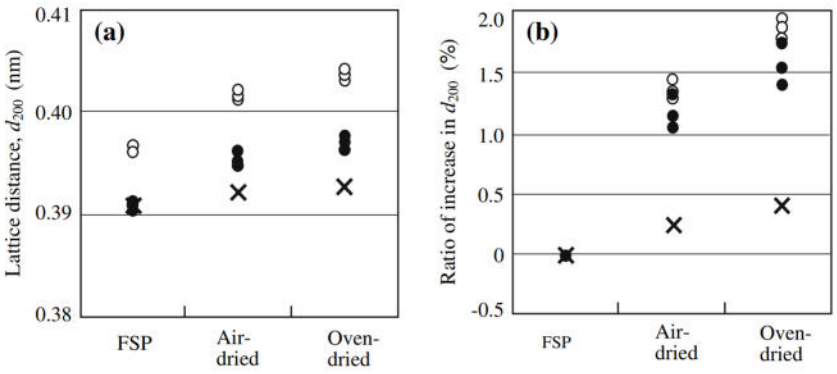

Fig. 8 **a** Lattice distance in the [200] plane (d_{200}) for normal and tension wood powders, and G-layer powder under various moisture conditions. **b** Ratio of increase in d_{200} in normal and tension wood powders, and G-layer powder under various moisture conditions, calculated on the basis of d_{200} at the FSP. *Filled circle* tension wood powders, *open circle* normal wood powders, *cross* powder of isolated G-layer

wall, indicating that the shift of apparent peak position of [200] overestimates the real one by 9%. However, it is considered that this overestimation is not so big to give an essential effect on the qualitative interpretation of behavior of cellulose in the cell wall as it dries. Moreover, it was considered that the halo peak from water does not give an intrinsic effect on the value of β, because the halo peak from bound water becomes quite broader as compared with the peak from [200] plane in the moisture content region less than the FSP.

Discussion

In the present study, it was shown that the ratio of increase in the longitudinal Young's modulus with drying was higher in the G-layer than in the L-layer, a pattern repeated with longitudinal drying shrinkage. Thus, it was concluded that the increased Young's modulus with drying in the G-layer compared to the L-layer causes the large increase in the Young's modulus of tension wood after drying. It was also concluded that an abnormally large shrinkage with drying in the G-layer compared to the L-layer causes the large shrinkage in the drying tension wood. By the way, as mentioned above, transverse sectioning often causes an artefactual swelling in the crosscut shapes of the G-layer, resulting in an overestimation of the values of g and γ (Clair et al. 2005b). This could lead to an underestimation of the differences in the physical properties between the G-layer and the L-layer. However, it is considered that the obtained conclusion is not disturbed by such an artifact because difference of the properties between the G- and the L-layers would be even greater if the possible overestimation of g and γ was taken into consideration.

It was also discovered that the lattice distance in the [200] plane (d_{200}) increased with drying, while the width of a single crystallite (*WSC*) in the direction

perpendicular to the [200] plane became smaller after drying, which is especially noticeably in the tension wood. The latter result comes from the increase in the half width of the [200] diffraction peak (β) with drying. Lately, Clair et al. (2008) showed that the tension wood cell wall has a gel-like structure characterized by a pore surface more than 30 times higher by analyzing nitrogen adsorption–desorption isotherms of supercritically dried tension and normal wood. Although the present results seem to be unrelated, the origin of these complex phenomena can be explained in the following manner via the gel-like structure of the tension wood cell wall proposed by Clair et al. (2008).

The G-layer matrix consists of a substantial amount of non-crystalline polysaccharides (NCPs), which in the green state, behaves like a water-swollen gel. During water desorption, the swollen gel of the NCPs collapses under surface tension. As a result, the matrix is transformed into a condensed structure by strong hydrogen bonding between NCP molecules, which is a form of xero-gelation, leading to an abnormal increase in the Young's modulus and high shrinkage in the drying G-layer. It is considered that the NCPs consist of small amounts of hemicelluloses besides non-crystalline cellulose, e.g., galactan, xyloglucan, and so forth (Norberg and Meier 1966; Nishikubo et al. 2007). According to Nishikubo et al. (2007), most of the non-cellulosic polysaccharide consists of xyloglucan, therefore, it is considered that xyloglucan might have an important role to control the mechanical behaviors of G-layer.

Lately, Fang et al. (2007) reported that relative thickness of G-layer became significantly smaller than that of the lignified layer after drying; moreover, lumen size in G-fiber increased while that in the N-fiber it decreased after drying. Their discovery suggests a possibility that a tensile stress is generated in the dried G-layer not only in the longitudinal but also in the circumferential directions. In other words, it is considered that some cellulose microfibrils in the dried G-layer are subject to transverse tensile and longitudinal buckling stresses from the shrinking NCP matrix. The combined effect causes disarray in the cellulose lattice arrangements, especially at the surface layer of each crystallite, which may cause an increase of β and thus an apparent decrease of *WSC* after drying. This may explain why d_{200} increases while *WSC* decreases in the dried G-layer. The possibility of longitudinal buckling in cellulose crystallites was also noted by Clair et al. (2006). Considering this anisotropic structure of cellulose crystallite, transverse stiffness is relatively lower in the direction perpendicular to the [200] lattice plane than in the direction along *b*-axis in the unit cell, possibly causing each crystallite more easily to deform or delaminate in the direction perpendicular to the [200] lattice plane than in the direction along *b*-axis under external negative pressure.

In the L-layer matrix, NCP molecules are reinforced by large amounts of lignin whose rigidity is higher than that of the NCPs under wet condition (Cousins 1976, 1978). As with the NCP matrix in the G-layer, the NCP domain in the green, lignified cell wall collapses with moisture desorption; however, its condensation and resulting xero-gelation is mechanically prevented by the lignin, which acts as a rigid skeleton in the matrix (Salmén and Olsson 1998; Akerholm and Salmén 2003). Thus, the ratio of increase in the longitudinal Young's modulus with drying is lower

in the L-layer than in the G-layer; longitudinal drying shrinkage also displayed a similar pattern of behavior. The increases in β values (and decrease in *WSC*) were thus lower in the L-layer than in the G-layer.

Conclusion

In the present study, the authors focused on the moisture-dependent changes in the longitudinal Young's modulus and longitudinal shrinkage in tension wood of Kunugi oak (*Quercus acutissima*), revealing the property difference between the G-layer and the L-layer. Moreover, the effect of moisture desorption on the behavior of cellulose crystallites in G-layer and L-layer was measured. Based on the obtained results, the following conclusion was derived.

In the green state, the polysaccharide matrix in the G-layer behaves as a water-swollen gel; however, it is transformed into a condensed and hard-packed structure by strong surface tension during moisture desorption, which is a form of xero-gelation. On the other hand, in the L-layer, condensation and subsequent xero-gelation of the polysaccharide matrix was prevented by the hydrophobic lignin that mechanically reinforces the matrix. Thus, the increased Young's modulus with drying in the G-layer compared to the L-layer causes the large increase in the Young's modulus of tension wood after drying. An abnormally large shrinkage with drying in the G-layer compared to the L-layer generates the large shrinkage in the dried tension wood.

References

Abe K, Yamamoto H (2005) Mechanical interaction between cellulose microfibril and matrix substance in wood cell wall determined by X-ray diffraction. J Wood Sci 51:334–338

Abe K, Yamamoto H (2006) Behavior of the cellulose microfibril in shrinking woods. J Wood Sci 52:15–19

Abe K, Yamamoto H (2007) The influence of boiling and drying treatments on the behaviors of tension wood with gelatinous layers in *Zelkova serrata*. J Wood Sci 53:5–10

Akerholm M, Salmén L (2003) The oriented structure of lignin and its viscoelastic properties studied by static and dynamic FT-IR spectroscopy. Holzforschung 57:459–465

Boyd JD (1977) Relationship between fiber morphology and shrinkage of wood. Wood Sic Technol 11:3–22

Clair B, Thibaut B (2001) Shrinkage of the gelatinous layer of poplar and beech tension wood. IAWA J 22:121–131

Clair B, Ruelle J, Thibaut B (2003) Relationship between growth stress, mechanical- physical properties and proportion of fibre with gelatinous layer in chestnut (Castanea sativa Mill). Holzforschung 57:189–195

Clair B, Thibaut B, Sugiyama J (2005a) On the detachment of the gelatinous layer in tension wood fiber. J Wood Sci 51:218–221

Clair B, Gril J, Baba K, Thibaut T, Sugiyama J (2005b) Precautions for the structural analysis of the gelatinous layer in tension wood. IAWA J 26:189–196

Clair B, Almeras T, Yamamoto H, Okuyama T, Sugiyama J (2006) Mechanical Behavior of cellulose microfibrils in tension wood, in relation with maturation stress generation. Biophys J 91:1128–1135

Clair B, Gril J, Di Renzo F, Yamamoto H, Quignard F (2008) Characterization of a gel in the cell wall to elucidate the paradoxical shrinkage of tension wood. Biomacromolecules 9:494–498

Cousins WJ (1976) Elastic modulus of lignin as related to moisture content. Wood Sci Technol 10:9–17
Cousins WJ (1978) Young's modulus of hemicellulose as related to moisture content. Wood Sci Technol 12:161–167
Fang CH, Clair B, Gril J, Almeras T (2007) Transverse shrinkage in G-fibers as the function of cell wall layering and growth strain. Wood Sci Technol 41:659–671
Fang CH, Clair B, Gril J, Liu SQ (2008) Growth stresses are highly controlled by the amount of G-layer in poplar tension wood. IAWA J 29:237–246
Hengstenberg J, Mark H (1928) Röntgenuntersuchungen über den Bau der C-Ketten in Kohlenwasserstoffen. Z Krist 67:583
Kojima Y, Yamamoto H (2004) Properties of the cell wall constituents in relation to the longitudinal elasticity of wood—Part 2. Origin of the moisture dependency of the longitudinal elasticity of wood. Wood Sci Technol 37:427–434
Kollmann F, Krech H (1960) Dynamic measurement of damping capacity and elastic properties of wood. Holz Roh Werkst 18:41–54
Kubler H (1987) Growth stresses in trees and related wood properties. For Prod Abs 10:62–118
Nishikubo N, Awano T, Banasiak A, Bouquin V, Ibatullin F, Funada R, Brumer H, Teeri TT, Hayashi T, Sundberg B, Mellerowicz EJ (2007) Xyloglucan end-transglycosylase (XET) functions in gelatinous layer of tension wood fiber in Poplar—a glimpse into the mechanism of the balancing act of trees. Plant Cell Physiol 48:843–855
Nishimura H, Okano T, Asano I (1981) Fine structure of wood cell wall. 1. Structural features of noncrystalline substances in wood cell wall. Mokuzai Gakkaishi 27:611–617
Norberg H, Meier H (1966) Physical and chemical properties of the gelatinous layer in tension wood fibres of aspen (*Populus tremula* L.). Holzforschung 6:174–178
Okuyama T, Yamamoto H, Iguchi M, Yoshida M (1990) Generation process of growth stresses in cell walls. II. Growth stress in tension wood. Mokuzai Gakkaishi 36:797–803
Okuyama T, Yamamoto H, Yoshida M, Hattori Y, Archer RR (1994) Growth stresses in tension wood. Role of microfibrils and lignification. Ann Sci For 51:291–300
Okuyama T, Doldan J, Yamamoto H, Ona T (2004) Heart splitting at crosscutting of *Eucalyptus grandis* logs. J Wood Sci 50:1–6
Onaka F (1949) Study on reaction wood. Wood Res (Bull Wood Res Inst Kyoto Univ) 1:1–99
Panshin AJ, de Zeeuw C (1971) Textbook of wood technology, 3rd edn. McGraw-Hill, New York
Salmén L, Olsson AM (1998) Interaction between hemicellulose, lignin and cellulose: structure-property relationships. J Pulp Paper Sci 24:99–103
Wilson B, Archer RR (1979) Tree design—some biological solutions to mechanical problems. Bioscience 29:293–298
Yamamoto H (1998) Generation mechanism of growth stresses in wood cell walls: roles of lignin deposition and cellulose microfibril during cell wall maturation. Wood Sci Technol 32:171–182
Yamamoto H (2004) Role of the gelatinous layer on the origin of the physical properties of the tension wood. J Wood Sci 50:197–208
Yamamoto H, Okuyama T, Sugiyama K, Yoshida M (1992) Generation process of growth stresses in cell walls. IV. Action of the cellulose microfibrils upon the generation of the tensile stresses. Mokuzai Gakkaishi 38:107–113
Yamamoto H, Okuyama T, Yoshida M (1993) Generation process of growth stresses in cell walls. V. Model of tensile stress generation in gelatinous fibers. Mokuzai Gakkaishi 39:118–125
Yamamoto H, Yoshida M, Okuyama T (2002) Growth stress controls negative gravitropism in woody plant stems. Planta 216:280–292
Yamamoto H, Abe K, Arakawa Y, Okuyama T, Gril J (2005) Role of the gelatinous layer (G-layer) on the origin of the physical properties of the tension wood of *Acer sieboldianum*. J Wood Sci 51:222–233
Yoshida M, Okuda T, Okuyama T (2000) Tension wood and growth stress induced by artificial inclination in *Liriodendron tulipifera* Linn. and Prunus spachiana Kitamura f. ascendens Kitamura. Ann For Sci 57:739–746
Yoshida M, Ohta H, Okuyama T (2002) Tensile growth stress and lignin distribution in the cell walls of black locust (*Robinia pseudoacacia*). J Wood Sci 48:99–105